JOURNAL OF MATERIALS SCIENCE 31 (1996) 4591–4598

The role of volatile solute elements in directed melt oxidation of aluminium alloys

V. JAYARAM
Department of Metallurgy, Indian Institute of Science, Bangalore 560 012, India

Surface oxide microstructures have been examined on composites prepared by directed melt oxidation of Al–Mg-based alloys. Evidence has been found that the pick-up of oxygen occurs by vapour-phase oxidation of magnesium to magnesium oxide, which is subsequently reduced to form alumina in a cyclic process. It is shown that other volatile elements, such as lithium, sodium and zinc result in the formation of solute-rich oxides whose stability may also be brought about by vapour enrichment. In all the above cases it was found that alumina matrix composites form beneath the surface (though the magnitude is small in the case of sodium). A comparison is made of the different types of oxidation behaviour among various systems that contain volatile solutes, i.e. Al–Mg, Al–Zn, Al–Li and Al–Na.

1. Introduction

The process of directed metal oxidation (DIMOX), that is now reported extensively in the open literature (see, for example, [1–9]), has been studied primarily on aluminium alloys that contain magnesium. These include Al–Mg, Al–Mg–Si, Al–Zn–Mg–Si and commercial aluminium alloys that contain, in addition to magnesium, other elements such as iron and copper. Microstructural characterization of the near-surface region has established that magnesium-containing oxides dominate the oxidation behaviour during incubation and growth. In the alloys that have been used, the thermodynamically stable oxide in equilibrium with the melt is spinel, $MgAl_2O_4$ (while this conclusion can, strictly speaking, only be reached for Al–Mg and Al–Mg–Si, it is unlikely that the other elements would, in the amounts that are usually present, bring about a significant change in the phase stability). It has, however, been argued that MgO is metastable when in direct contact with the melt and that this microstructure can sustain the growth of alumina by a two-step process (Fig. 1) wherein dissolution of the MgO at the MgO/alloy interface contributes oxygen for the formation of alumina, while the magnesium that is released is transported through the MgO layer to the outer interface with the atmosphere, either by ionic transport or through the vapour phase [8, 9]. Thus, alumina is formed subsurface at the liquid–Al_2O_3 interface, thereby leading to the growth of monocrystalline columns with [0001] close to the surface normal. Periodically, spinel forms at this MgO/Al interface, owing to fluctuations in the magnesium concentration in the melt [9] and this spinel can itself undergo kinetic de-mixing [3] so that the MgO on the surface is always present (Fig. 1).

Some of the issues that continue to remain unclear include the following. (i) Is MgO continuously formed by diffusion of cations or by a vapour-phase mechanism? (ii) Is the growth of Al_2O_3 determined by diffusional transport of charged species across this layer of MgO? (iii) Are there other elements which can substitute for magnesium in promoting the oxidative growth of alumina?

For example, in relation to (iii), it has been asserted [6] that Al–Zn alloys will oxidize only when at least trace amounts of magnesium are present to create a surface layer of MgO, while Al–10Si–3Zn–0.2Mg alloys have been shown to grow with ZnO on the surface [7] but it is once again assumed that it is diffusive transport of charged species across ZnO that determines the growth of alumina.

In order to address some of these issues, the microstructure at the surface of composites grown from Al–Mg–Si alloys was examined carefully by TEM. Based on indications that vapour-phase oxidation may be taking place, it was decided to attempt oxidation on other binary systems using solute elements, sodium, lithium and zinc, with high vapour pressures. As will be seen later, all of these alloy systems display growth of alumina/alloy composite. The likely mechanisms that promote growth are discussed in terms of the relevant phase equilibria and solute vapour pressure.

2. Experimental procedure

Al–Mg–Si alloys, previously prepared and oxidized to form composites (see [3]), were coated with chromium, sectioned and made into TEM specimens. The intention of the evaporated chromium was to define the surface unambiguously in the TEM. Samples were extracted from the furnace at the process temperature to minimize microstructural changes during cooling.

0022–2461

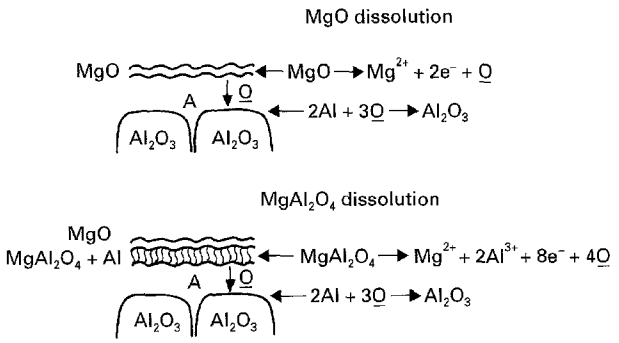

Figure 1 Schematic illustration of surface layers indicating the decomposition of MgO or $MgAl_2O_4$ at the interface with the alloy. From Salas *et al.* [9].

Binary Al–Na, Al–Li, and Al–Zn alloys were prepared by melting pure elements in a resistively heated furnace and were cast into moulds. Nominal and actual compositions are given in Table I. All alloys were ground on 600 grit SiC and degreased in ethanol before the experiment.

Oxidation experiments on Al–Na/Li/Zn were carried out at 1050 °C in alumina tubes, the bottom ends of which were covered with an alumina disc and bonded with refractory alumina cement. No reaction could be observed between the alloy and the cement after the experiment. Heating rates of $\sim 40\,^{\circ}C\,min^{-1}$ were employed in an air furnace equipped with molybdenum disilicide heating elements. After various soak times, the samples were cooled and characterized by optical microscopy, SEM and X-ray diffraction (XRD). TEM was carried out in a Jeol 2000 FX equipped with a Tracor-Northern EDS System. Some runs were carried out in a thermogravimetric analyser (TGA) in order to obtain an idea of growth kinetics.

3. Results

3.1. Al–Mg–Si

Earlier observations [3] have suggested the existence of sequential layers of MgO, $MgAl_2O_4$ and aluminium as shown schematically in Fig. 1. In the present experiments, two additional types of microstructure were found. The image in Fig. 2a comes from a near-surface region showing alternating twins T_1 and T_2 of MgO with adjoining aluminium channels that are perpendicular to the surface. The identification of the phases was carried out by microdiffraction and X-ray analysis. A lattice resolution image of the interface between aluminium and MgO is shown in Fig. 2c. The beam direction is along [1 1 0] MgO and the spacing of spots in the 30 nm interfacial region corresponds to the spacing expected in a [1 1 0] structure image of $MgAl_2O_4$. Thus, a combination of lattice imaging and selected-area diffraction indicates that $MgAl_2O_4$ has formed as an epitaxial layer on the MgO. Notice that the lattice planes in the spinel are reflected about the arrowed direction which corresponds to the projection of {1 1 1}. Thus, the same twins that are seen in the MgO of Fig. 2b are reproduced in the spinel, suggesting that the latter evolved out of an interfacial reaction between the melt and the MgO. (Both oxides have an f c c arrangement of anions and the epitaxial relationship is therefore expected in such a reaction). An example of the second and more common observation is illustrated in Fig. 3. The region marked A in Fig. 3a is a mixture of alloy and MgO with some spinel. This distribution of phases that was confirmed by diffraction (Fig. 3b) is seen entirely within the alumina grain which is well known to be monocrystalline over tens or hundreds of micrometres. Thus, the MgO is at one point in time interspersed in the alloy channel as fine particles and subsequently appears to react to form alumina.

TABLE I Composition (at %) of alloys used for oxidation

	Nominal	Actual
Zn	2.1	2.1
Na	3.5	3.2
Li	–	5.5

Such observations may also be made on cross-sections in the SEM as illustrated by the image and X-ray maps in Fig. 4 which show magnesium-rich surfaces on top of Al_2O_3–Al composite. The dark portions in region X of the image correspond to metal, while the "grains" distributed within are $MgO/MgAl_2O_4$. Many such regions display such a microstructure which may now be interpreted as $Al + MgO/MgAl_2O_4$ in the light of the crystallographic and microchemical data obtained in the TEM.

Given the presence of aluminium within the MgO, the proximity of the metal to the surface may be studied by Auger spectroscopy (Charles Evans & Assoc. Redwood City, CA, USA) as shown in Fig. 5. A typical spectrum on the as-received surface is shown in Fig. 5a while Fig. 5b displays the peak–peak height variation after sputtering a $300 \times 300\ \mu m$ area with 4 KeV N^+ ions for various times. (The sputtering rates were calibrated with a SiO_2 thin film.) Quantification of data to yield compositions proved unreliable owing to the rough surface. The surface aluminium signal might arise from either $MgAl_2O_4$ or alloy, but the presence of silicon, which is only found in elemental form, strongly suggests the presence of alloy within 2 nm of the free surface. Notice also that the rise in the aluminium signal after 11 min and 300 nm sputtering, coincides with a drop in the oxygen signal, suggesting the presence of unoxidized aluminium within this layer.

3.2. Al–Na, Al–Li, Al–Zn

Fig. 6 displays the weight gain for different alloys at the given temperatures and oxidation times. Alumina matrix composites were found to grow on all three alloys but the weight gained by Al–Na corresponded to the growth of only a few hundred micrometres after which the rate of oxidation became negligible. The rapid initial rate of oxidation, the subsequent drop and the development of oscillations in the growth of composite from Al–Li, are similar to the behaviour of binary Al–Mg alloys [9].

X-ray diffraction and chemical analysis by flame photometry of scrapings from the surface enable the principal phases on the surface to be identified as tabulated in Table II. The presence of zinc and sodium on the surface was also confirmed by SEM/EDS. Theoretical weight fractions of sodium and lithium in selected mixed oxides are also given for comparison in Table II.

4. Discussion

4.1. Al–Mg

The microstructures at the surface of composites made from Al–Mg–Si strongly suggest that (a) alloy phases, fine-grained MgO and $MgAl_2O_4$ can be intermingled, and that (b) $MgAl_2O_4$ can form as an interfacial reaction product between aluminium and MgO. These observations support the conclusion that MgO is initially in metastable equilibrium with the alloy and subsequently reacts by an exchange mechanism to form Al_2O_3 via the intermediate phase $MgAl_2O_4$. It is known [1, 5] that the channels in the composite that feed alloy from the reservoir to the surface contain low amounts of magnesium, typically 0.2–0.5% which represents the composition near the corner of the three-phase equilibrium (Al, Mg) + $MgAl_2O_4$ + Al_2O_3. Calculations of phase equilibria show that for MgO to be in equilibrium with the alloy, one requires at least 8% Mg [3] at 1100 °C. Thus, the most plausible explanation for the formation of MgO is by periodic vapour-phase enhancement of the concentration of magnesium at the melt–air interface.

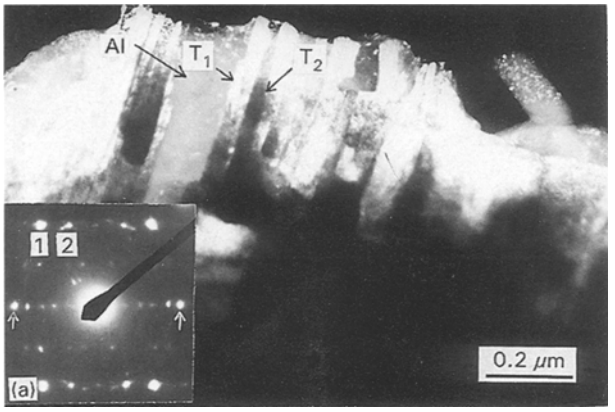

Figure 2 (a) Dark-field micrograph using a twin reflection of the near-surface region showing twinned MgO (T_1, T_2) and alloy channels (A1) running normal to the surface. The inset shows a selected-area diffraction pattern along [1 1 0] with the (1 1 1) twin plane arrowed. Two ***g***-vectors of the type 1 1 1 and 2 0 0 that are twin related are indicated by 1, 2. They are also found in positions that are reflected across the normal to the twin plane. (b) Lattice image of the interface between alloy and MgO in (a) showing the presence of about 200 nm thick spinel layer. Note the twin interface in the spinel (arrowed), similar to that in MgO in (a). The beam direction is [1 1 0] of both MgO as well as of the spinel but the MgO structure is not resolved.

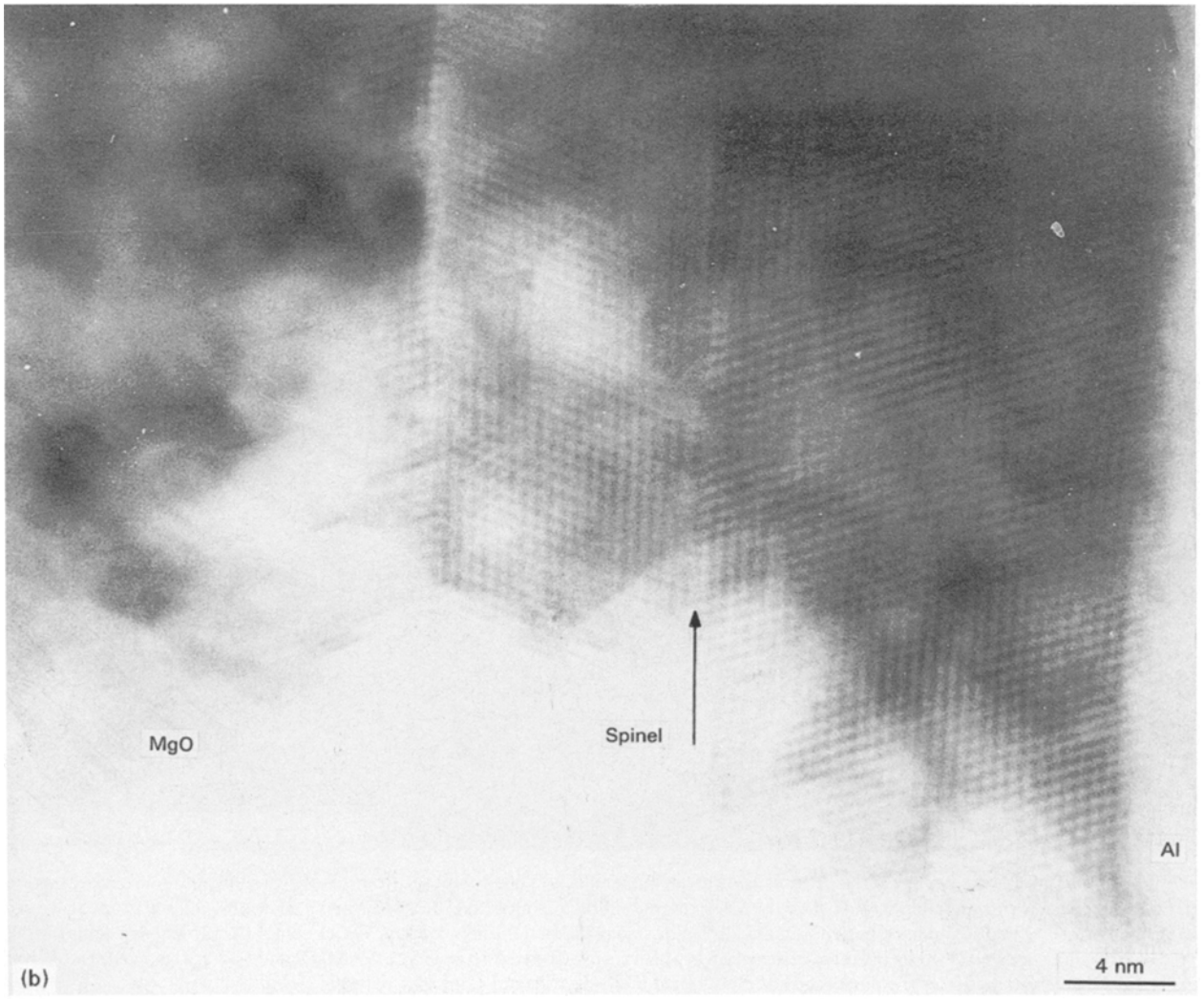

The above argument may also be extended to Al–Zn alloys for which it is readily shown from free energy data that ZnO cannot be in stable equilibrium with the melt unless the mole fraction of zinc reaches close to unity. For Al–Li and Al–Na alloys, the surface oxides that are experimentally seen on the growing Al_2O_3–Al composite are $LiAlO_2$ and $NaAlO_2$. As shown in Appendix 1, the high free-energy of formation of $LiAlO_2$ [10, 11] from Li_2O and Al_2O_3 ensures its stability over the greater part of the phase diagram. In the case of Al–Na, immiscibility in the liquid phase [12] leads to the stabilization of various mixed oxides in preference to Al_2O_3 and while there is no evidence to prefer $NaAlO_2$, its presence is not inconsistent with possible phase equilibria (Fig. 7). Thus, though the evidence is compatible with vapour-phase enrichment of sodium and lithium, it is not as compelling as in the case of magnesium and zinc. The alternative mechanism of oxygen intake by diffusion of cation vacancies through MgO may well also operate but, as shown in

Figure 3 (a) Dark-field image of the surface region using an alumina reflection of a composite from Al–Mg–Si showing a fine microstructure (arrowed) interspersed in alumina "grains" (A). (b) Selected-area diffraction from (a). Because MgO and $MgAl_2O_4$ are f c c with lattice parameters of ~0.42 and 0.81 nm, respectively, many of the low-index diffraction rings overlap. The existence of both polycrystalline MgO and $MgAl_2O_4$ may be established by the three-arrowed rings which correspond to 4 4 0 (spinel), 2 2 0 (MgO) and 3 3 3/5 1 1 (spinel). The Al and Al_2O_3 are single crystalline over the dimensions of the selected-area aperture and yield spot patterns.

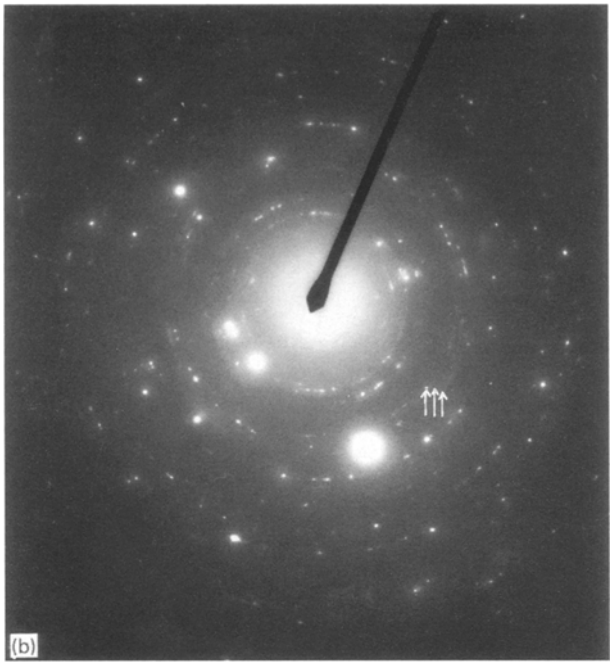

Figure 3 (Continued)

Appendix 2, it is unlikely to be able to generate the flux necessary to sustain the experimental growth rates.

A final observation may be made with regard to the differences in the rates of growth of composites from these four binary alloys. While all of them show a tendency to decelerate with increasing composite thickness [4, 13], Al–Na alloys cease to grow after barely 200 μm of composite. A related observation has been made on aluminium seeded with NaOH before oxidation [14]. The abrupt termination of growth was ascribed to significant loss of sodium by vaporization. An alternative explanation in the present case may lie in the fact that it may not be possible to maintain equilibrium between Al–Na and Al_2O_3 in the presence of any reasonable amount of sodium owing to the high activity of sodium (given the reported immiscibility in the liquid at lower temperatures).

5. Conclusion

There is strong evidence to suggest that the mechanism by which oxygen is absorbed during oxidative

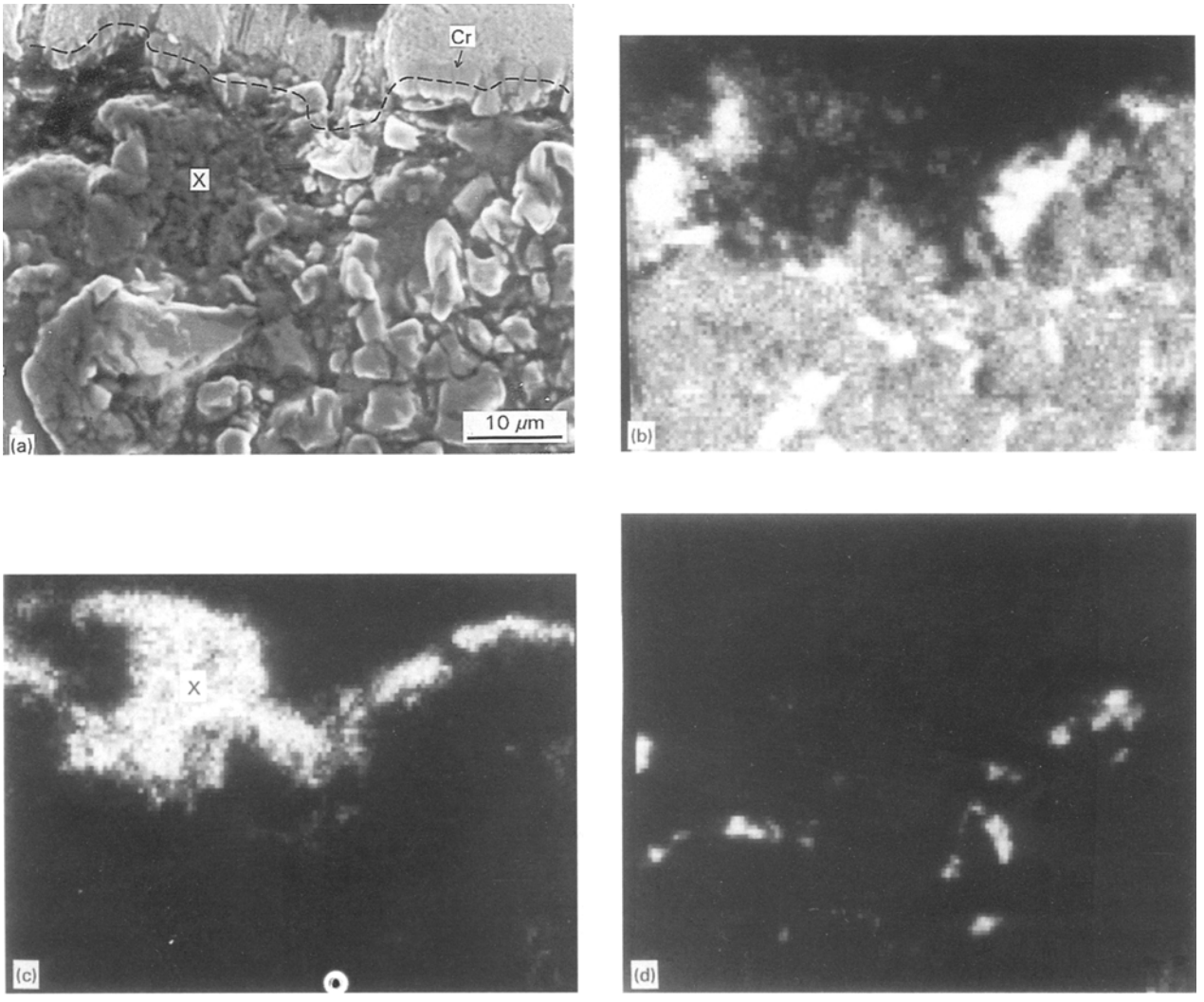

Figure 4 (a) Secondary electron image and (b–e) X-ray maps of the surface of a composite, showing the same field of view. Notice the large expanse at the top left (X) showing "particles" in a matrix. The dark contrast is characteristic of metal while the bright regions are magnesium-containing oxide. The chromium layer is shown dashed in (a), and as seen in the chromium X-ray map in (b–e), serves to define the positions of other elements with respect to the surface. (b) Al, (c) Mg, (d) Si, (e) Cr.

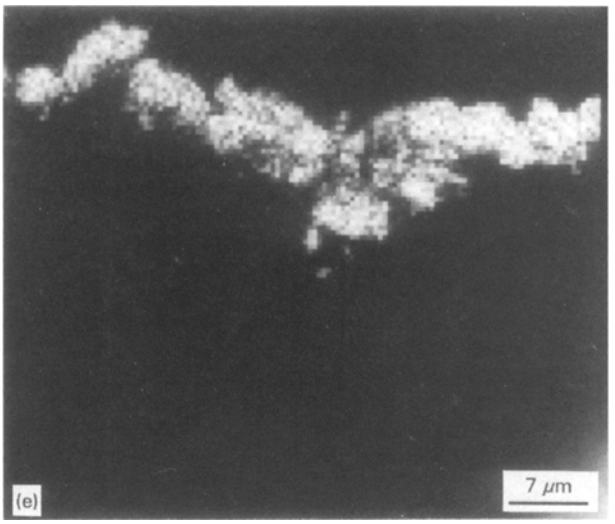

Figure 4 (Continued)

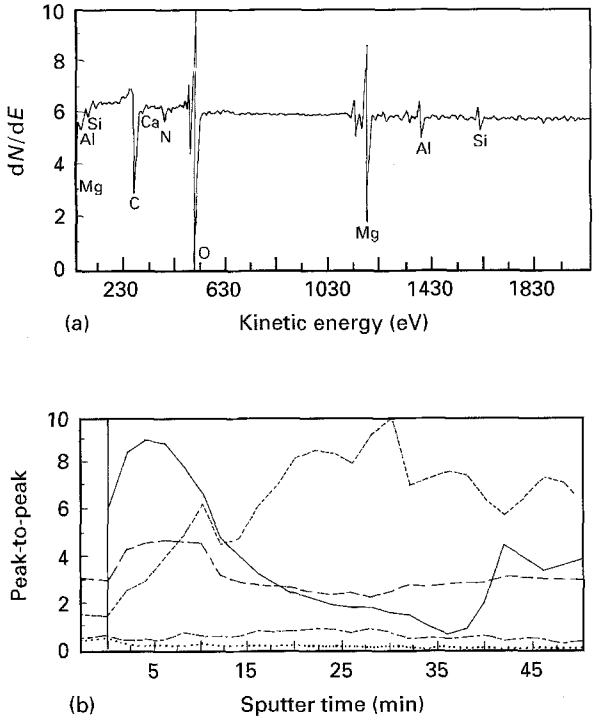

Figure 5 (a) Auger spectrum of as-received surface indicating the presence of aluminium, magnesium, silicon and oxygen. (b) Depth profile for various elements after N^+ sputtering at 25 nm min^{-1}. (---) A 12, (——) Mg 2, (---) O 1, (—·—) S 12, (···) C 1.

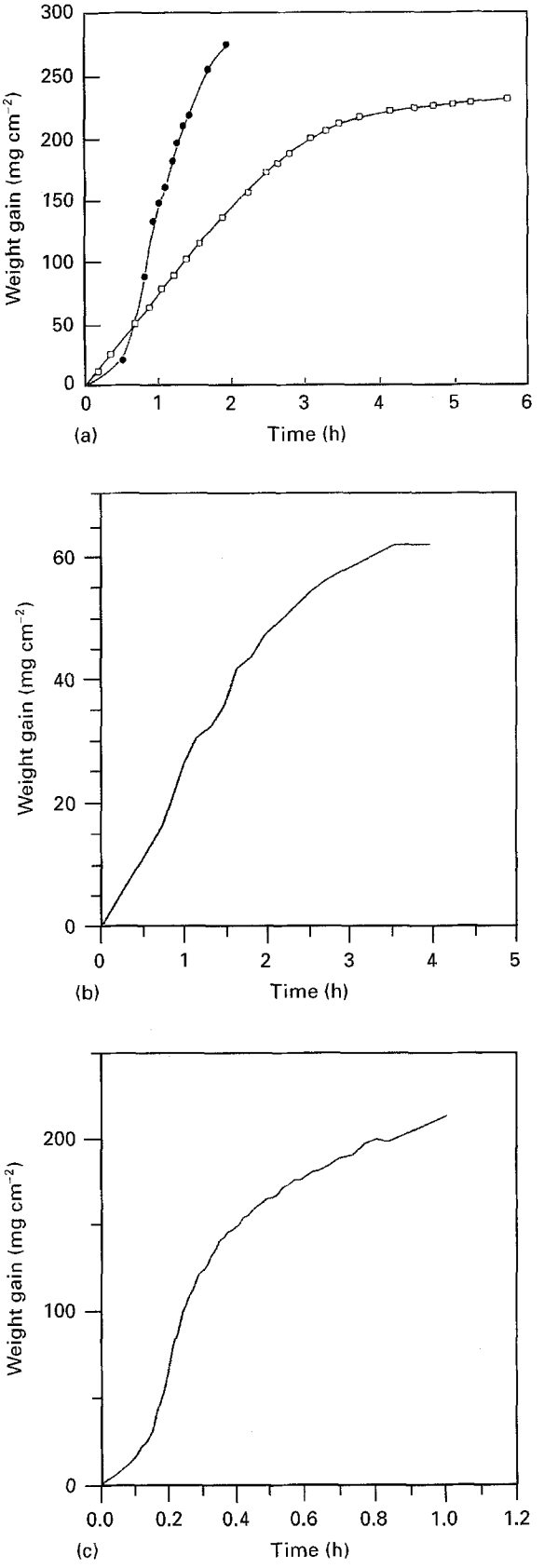

Figure 6 Weight gain versus time for (a) Al–Zn (1050 °C), (b) Al–Na (1100 °C) and (c) Al–Li (1100 °C) alloys. (a) (●) Al–5Zn–0.3Mg, (□) Al–5Zn. Notice that the slope in (c) periodically fluctuates after 0.3 h, indicating an oscillatory rate of weight gain.

growth of Al_2O_3–Al composites from Al–Mg and Al–Zn based alloys is through vapour-phase oxidation of the solute species. Growth of the bulk Al_2O_3–Al composite would then proceed by cyclic dissolution of this oxide (ZnO, MgO) into the melt to form Al_2O_3 by an exchange reaction. This sequence of events can also lead to the observed epitaxial columnar growth of Al_2O_3 but does not require diffusion of species (whether electronic or ionic) across the surface oxide. It does, however, imply periodic microrupture of the surface film to allow vaporization of solute.

Acknowledgement

Funding for this work was provided to the Indian Institute of Science by the Aeronautical R and D Board and by the Department of Science and

TABLE II Characterization of surface oxide

	EDS	XRD	Wet chemical analysis (wt % solute)	Solute in selected oxides (wt %)
Al–Li	Al	γ-$LiAlO_2$	10.5	10.6 ($LiAlO_2$)
Al–Zn	Zn	ZnO	–	–
Al–Na	Na, Al	[a]	25.3	28.0 ($NaAlO_2$)

[a] Quantity insufficient for XRD.

Technology, Government of India. A part of the work was carried out with support from the Advanced Research Project Agency, USA at the University of California, Santa Barbara (UCSB). The author would like to acknowledge useful discussions with O. Salas, C. G. Levi and K. C. Vlach of UCSB and the experimental assistance of M. Hanabe, J. Michael and Rajan Ambat.

Appendix 1

To determine the compositions of the alloys in simultaneous equilibrium with Al_2O_3 and a mixed oxide, one can write

$$M(Na, Li) + (n + \tfrac{1}{3})\tfrac{1}{2}Al_2O_3 = \tfrac{1}{2}[M_2O \cdot nAl_2O_3] + \tfrac{1}{3}Al \quad (A1)$$

$$G^0 = \tfrac{1}{2}[G_f^0(M_2O \cdot nAl_2O_3 - (n + \tfrac{1}{3})G_f^0(Al_2O_3)] \quad (A2)$$

In addition, for the reaction

$$M_2O + nAl_2O_3 \rightarrow M_2O \cdot nAl_2O_3 \quad (A3)$$

$$G_r = G_f^0(M_2O \cdot nAl_2O_3) - G_f^0(M_2O) - nG_f^0(Al_2O_3) \quad (A4)$$

Therefore

$$G^0 = \tfrac{1}{2}[G_r + G_f^0(M_2O) - \tfrac{1}{3}G_f^0(Al_2O_3)] \quad (A5)$$

At equilibrium

$$-RT\ln(a_{Al}^{1/3}/a_M) = G^0 \quad (A6)$$

At 1300 K

$$G_f^0(Li_2O) = -426\ kJ\ mol^{-1} \quad (A7)$$

For solute-rich mixed oxide to be more thermodynamically stable than α-Al_2O_3, we require

$$G^0 < -RT\ln(a_{Al}^{1/3}/a_M) \quad (A8)$$

For Al–5% Li, by a similar analysis, one obtains

$$G_r < -56.4\ kJ\ mol^{-1}$$

From Kubaschewski [10], $G_r(Li_2Al_2O_4)$ may be obtained by extrapolation to be $\sim 135\ kJ\ mol^{-1}$, thus indicating that the mixed oxide is substantially favoured. The values of free energy used here give a composition of 0.5% Li in simultaneous equilibrium with $Li_2Al_2O_4$ and Al_2O_4, which is consistent with recently published calculations [15] where 0.13% Li was found to be in equilibrium with both oxides at 1000 K.

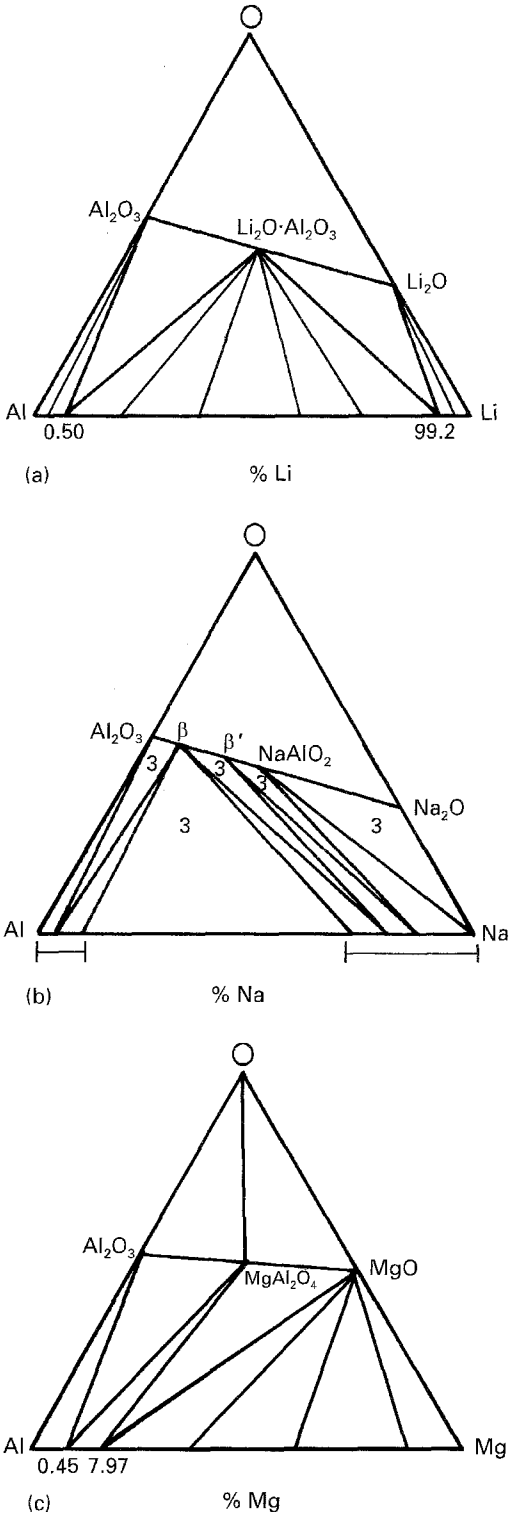

Figure 7 Ternary isothermal sections illustrating equilibria between oxides and liquid alloy for Al–Li, Al–Na and Al–Mg. For Al–Na the phase fields are schematically shown based on Jacob *et al.* [12]. Solubilities in the liquid, denoted by the ranges ⊢⊣, are, in practice, close to zero, owing to immiscibility. Two-phase regions in Al–Li–O are indicated by light lines. In Al–Na–O, "3" indicates three-phase fields, while others are two-phase fields. (a) 1300 K, (b) 1173 K, (c) 1373 K.

Appendix 2

There is another argument that sugggests that the diffusion of ionic species, such as magnesium vacancies, are unlikely to be rate-controlling. A typical growth rate for Al–Mg–Si alloys at 1100 °C is

$\sim 10^{-5}\,\mathrm{cm\,s^{-1}}$. This requires a flux of oxygen ions/magnesium ions of $\sim 10^{-6}\,\mathrm{mol\,cm^{-2}\,s^{-1}}$.

Thus, $DC/X \simeq 10^{-6}$, where C is a concentration difference and x is a diffusion length.

A typical lattice diffusivity for Mg^{2+} in MgO is $-10^{-12}\,\mathrm{cm^2\,s^{-1}}$ at 1100 °C [16]. Note that it has been reported that, unlike oxygen ions, cations are not more mobile along grain boundaries. Thus, $C/X = 10^{6}\,\mathrm{mol\,cm^{-4}}$.

Even if the oxide thickness was only 10 nm, there must exist a concentration difference, C, of about $1\,\mathrm{mol\,cm^{-3}}$. This is manifestly unreasonable, given that the molar density of Mg^{2+} in MgO is only $\simeq 0.1\,\mathrm{cm^{-3}}$. Thus, the requirement of rapid diffusion is probably met by pores, whereupon the pertinent parameter is the gas-phase diffusivity of magnesium.

References

1. M. S. NEWKIRK, A. W. URQUHART, H. R. ZWICKER and E. BREVAL, *J. Mater. Res.* **1** (1986) 81.
2. M. S. NEWKIRK, H. D. LESHER, D. R. WHITE, C. R. KENNEDY, A. W. URQUHART and T. D. CLAAR, *Ceram. Engng. Sci. Proc.* **8** (1987) 879.
3. O. SALAS, H. NI, V. JAYARAM, K. C. VLACH, C. G. LEVI and R. MEHRABIAN, *J. Mater. Res.* **6** (1991) 1964.
4. K. C. VLACH, O. SALAS, H. NI, V. JAYARAM, C. G. LEVI and R. MEHRABIAN, *ibid.* **6** (1991) 1982.
5. E. BREVAL, M. K. AGHAJANIAN and S. J. LUSZCZ, *J. Am. Ceram. Soc.* **73** (1990) 2610.
6. M. SINDEL, N. A. TRAVITZKY and N. CLAUSSEN, *ibid.* **73** (1990) 2615.
7. A. S. NAGELBERG, *Solid State Ionics* **32/33** (1989) 783.
8. A. S. NAGELBERG, S. ANTOLIN and A. W. URQUHART, *J. Am. Ceram. Soc.* **75** (1992) 455.
9. O. SALAS, V. JAYARAM, K. C. VLACH, C. G. LEVI and R. MEHRABIAN, in "TMS Conference on Processing and Fabrication of Advanced Materials for High Temperature Applications", edited by V. A. Ravi and T. S. Srivatsan (The Minerals, Metals and Materials Society, Warrendale, PA, 1992) p. 143.
10. O. KUBASCHEWSKI, *High Temp. High Press.* **4** (1972) 1.
11. "JANAF Thermochemical Tables", *J. Phys. Chem. Ref. Data*, Vol. 14 Supplement 1 (The American Chemical Society and American Institute of Physics for National Bureau of Standards, Washington, 1985).
12. K. T. JACOB, K. SWAMINATHAN and O. M. SREEDHARAN, *Electrochim. Acta* **36** (1991) 791.
13. O. SALAS, PhD thesis, University of California, Santa Barbara (1992).
14. P. XIAO and B. DERBY, *J. Am. Ceram. Soc.* **77** (1994) 1771.
15. D. A. WEIRAUCH and G. E. GRADDY, *ibid.* **65** (1992) 1484.
16. J. M. VIERIA and R. J. BROOK, in Advances in Ceramics, Vol. 10, "Structure and Properties of MgO and Al_2O_3 Ceramics", edited by W. D. Kingery (American Chemical Society, Columbus, OH, 1983) p. 438.

Received 17 March 1995
and accepted 13 February 1996